4056 *Chem. Mater.* **2010,** *22,* 4056–4061
DOI:10.1021/cm101058y

CHEMISTRY OF MATERIALS
Article

Electrochemical Synthesis of Catalytically Active Ru/RuO$_2$ Core−Shell Nanoparticles without Stabilizer

Bo Zhang, Changbin Zhang,* Hong He,* Yunbo Yu, Lian Wang, and Jie Zhang

State Key Laboratory of Environmental Chemistry and Ecotoxicology, Research Center for Eco-Environmental Sciences, Chinese Academy of Sciences, Beijing 100085, China

Received April 16, 2010. Revised Manuscript Received May 25, 2010

Ru/RuO$_2$ core−shell nanoparticles were synthesized by electrochemical method in water without the addition of stabilizers. The zeta potential of the fresh nanoparticles was 30.8 mV in pure water at 25 °C, confirming that the repulsion between the particles is strong enough to stabilize them in aqueous solution. When the Ru/RuO$_2$ nanoparticles were loaded on metal oxide supports (CeO$_2$, TiO$_2$ and Al$_2$O$_3$), the structure of Ru core and RuO$_2$ shell remained unchanged on CeO$_2$ support, whereas Ru core was preferred to be oxidized to RuO$_2$ on TiO$_2$ and Al$_2$O$_3$. The catalytic oxidations of ethanol were chosen to compare the catalytic properties of the Ru/RuO$_2$ nanoparticles supported catalysts (our method) with that of Ru catalysts prepared by traditional wet impregnation method. All catalysts prepared by our method showed higher catalytic activities for the catalytic oxidations of ethanol than the Ru catalysts prepared by wet impregnation.

1. Introduction

Nanosized ruthenium (Ru) and its oxides have been widely explored as catalysts, with promising results.[1] Until now, almost all inorganic Ru supported catalysts have been prepared by the impregnation technique which consists of the reduction and decomposition of the metal salts impregnated on the support's surface.[1] This technique, however, fails to effectively control the size and shape of the Ru nanoparticles, which are important factors for the activity of catalysts. The well-defined Ru nanoparticles have been prepared by reducing metal salts in solution with the protection of soft or hard stabilizers such as organic mediums[2,3a,3b] and carbon nanotubes.[3c,d] Supported catalyst can be obtained by the adsorption or grafting of the nanoparticle onto the support. During this process, the stabilizer should be removed because the residual stabilizer in catalyst will decrease the activity of the nanoparticles supported catalyst.[4] Unfortunately, the step of stabilizer removal generally results in the loss of well-defined size and shape of nanoparticle. Therefore, it is of great interest to develop a new synthetic strategy for preparation of the uniform Ru nanoparticles without the use of stabilizer.

One of the primary advantages of the electrochemical synthesis of metal nanoparticles (e.g., Pt, Au, Ag, Pd) is that inorganic salts can be reduced at the cathode, thereby avoiding contamination with the byproduct of chemical-reducing agents.[2,5] In this paper, monodispersed and stable Ru/RuO$_2$ core−shell nanoparticles have been first synthesized using an electrochemical method in water without the addition of stabilizing agents. In addition, Ru/RuO$_2$-supported catalysts prepared by the loading method had high activity for the catalytic oxidation of ethanol, which is important in the issue of fuel consumption and fuel alternatives.

2. Experimental Section

2.1. Materials. RuCl$_3$ was purchased from the Johnson Matthey Company in London. All chemicals were of analytical grade and ultrapure water was used. The electrolytic solution for the preparation of the Ru single crystals in 30 mL solution consisted of 5.0×10^{-4} mol dm^{-3} RuCl$_3$, 0.1 mol dm^{-3} KNO$_3$.

2.2. Electrochemical Synthesis of the Ru/RuO$_2$ Nanoparticles. The electrochemical synthesis of the Ru single crystals was first conducted in a three-electrode cell in a potentiostatic manner. A rotating platinum electrode, made from a 3.0 mm diameter platinum disk, was used as the cathode and the rotation speed

*Corresponding author. E-mail: cbzhang@rcees.ac.cn (C.Z.); honghe@rcees.ac.cn (H.H.). Phone: +86-10-62849123. Fax: +86-10-62923549.

(1) (a) Mitsui, T.; Tsutsui, K.; Matsui, T.; Kikuchi, R.; Eguchi, K. *Appl. Catal., B* **2008**, *81*, 56–63. Silva, A. M.; Barandas, A. P. M. G.; Costa, L. O. O.; Borges, L. E. P.; Mattos, L. V.; Noronha, F. B. *Catal. Today* **2007**, *129*, 297–304. (b) Zhu, Y.; Widjaja, E.; Shirley, L. P. S.; Wang, Z.; Carpenter, K.; Maguire, J. A.; Narayan, S. H.; Hawthorne, M. F. *J. Am. Chem. Soc*. **2007**, *129*, 6507–6512. Wang, Y.; Jacobi, K.; Schone, W. D.; Ertl, G. *J. Phys. Chem. B* **2005**, *109*, 7883–7893. Pinna, F.; Scarpa, M.; Strukul, G.; Guglielminotti, E.; Boccuzzi, F.; Manzoli, M. *J. Catal.* **2000**, *192*, 158–162.
(2) Pachón, L. D.; Rothenberg, G. *Appl. Organomet. Chem*. **2008**, *22*, 288–299.
(3) (a) Viau, G.; Brayner, R.; Poul, L.; Chakroune, N.; Lacaze, E.; Fievet-Vincent, F.; Fievet, F. *Chem. Mater*. **2003**, *15*, 486–494. (b) Wang, Y.; Ren, J.; Deng, K.; Gui, L.; Tang, Y. *Chem. Mater*. **2000**, *12*, 1622–1627. (c) Min, Y.-S.; Bae, E. J.; Jeong, K. S.; Cho, Y. J.; Lee, J.-H.; Choi, W. B.; Park, G.-S. *Adv. Mater*. **2003**, *15*, 1019–1022. (d) Chaturvedi, H.; Poler, J. C. *J. Phys. Chem. B* **2006**, *110*, 22387–22393. Bedford, N.; Dablemont, C.; Viau, G.; Chupas, P.; Petkov, V. *J. Phys. Chem. C* **2007**, *111*, 18214–18219.
(4) Narayanan, R.; El-Sayed, M. A. *J. Phys. Chem. B* **2005**, *109*, 12663–12676. Lee, H.; Habas, S. E.; Kweskin, S.; Butcher, D.; Somorjai, G. A.; Yang, P. *Angew. Chem., Int. Ed.* **2006**, *45*, 7824–7828.
(5) Reetz, M. T.; Helbig, W. *J. Am. Chem. Soc*. **1994**, *116*, 7401–7402.

 Published on Web 06/15/2010

of the cathode was maintained at 1,000 rpm. A saturated calomel electrode (SCE) and 1.0 cm ×0.5 mm platinum rod was used as the reference and counter electrode, respectively. The applied potential on the rotating electrode was −1.0 V versus SCE. The electrolytic solution was deaerated by bubbling ultrahigh purity Ar for 1 h before synthesis and the electrolysis was protected with an Ar atmosphere during the whole process. The electrochemical synthesis of the Ru single crystals was also carried out in a two-electrode cell. The results were the same as that of the three-electrode system when the applied potential was −0.92 V and the electrolytic time was 10 min. After the electrolysis, the Ru nanoparticles were ultrasonically dispersed in 40 mL water in atmosphere at room temperature to form RuO_2 shell covering the Ru nanoparticles. Finally, the Ru/RuO_2 nanoparticles were centrifuge-washed to remove other ions.

Voltammetric measurements were carried out with a CHI 660C electrochemical workstation. A 5.0 mm × 2.0 mm platinum plate was used as the working electrode. A saturated calomel electrode and 1.0 cm ×0.5 mm platinum rod was used as the reference and counter electrode, respectively.

2.3. Preparation of Catalysts. Three common oxides, TiO_2, Al_2O_3 and CeO_2 nanorods, were employed as supports. Anatase TiO_2 was purchased from the Shanghai Huijing Co. China. The AlOOH powder (surface area = 292.1 $m^2\ g^{-1}$) was calcined at 600 °C for 3 h in air to obtain the Al_2O_3. CeO_2 nanorods were prepared following the procedure of Zhou et al.[6] In summary, 10 mol L^{-1} NaOH solution was added to 0.7 mol L^{-1} cerium(III) chloride solution, with 30 min of stirring. The resultant slurry was then transferred into an autoclave. After about 12 h at 100 °C, the system was cooled to room temperature. The final product was collected by filtration, washed with deionized water to remove any possible ionic remnants, and was then dried at 60 °C and calcined at 350 °C for 4 h. Ru/RuO_2 nanoparticles were loaded on the above oxides via the rotary evaporation method at 50 °C. These catalysts (marked as Ru/CeO_2(re), Ru/TiO_2(re), and Ru/Al_2O_3(re)) were then air-dried at 100 °C for 10 h, which was followed by calcination at 300 °C for 3 h. The Ru supported catalysts were also prepared by the traditional impregnation method with $RuCl_3$ solution (marked with im, such as Ru/CeO_2 (im)) for later catalytic activity comparison.

2.4. Characterization of Ru/RuO_2 Nanoparticles and Catalysts. Transmission electron microscopy (TEM) photographs were taken with a Hitachi H-7500 electron microscope at an accelerating voltage of 80 kV. The crystalline structure and elemental analysis of the nanoparticles were characterized by a JEOL JEM-2010 field emission high-resolution electron transmission microscopy (HRTEM) equipped with EDS at an accelerating voltage of 200 kV. X-ray powder diffraction (XRD) measurements were obtained using a computerized Rigaku D/max-RB Diffractometer (Japan, Cu Kα radiation, 0.154056 nm). Scans were taken over a 2θ range of 10° to 90° at a speed of 4° min^{-1}. The accelerating voltage and the applied current were 40 kV and 300 mA, respectively. X-ray photoelectron spectroscopy (XPS) measurements were carried out on a PHI Quantera spectrometer (ULVAC-PHI, Inc.) using Al Kα radiation ($h\nu$ = 1486.7 eV). The binding energy was corrected by the contaminated carbon (284.6 eV). Surface cleaning of samples was done by 500 eV Ar^+. Prior to peak fitting, the curves were employed a Shirley-type background. Electrophoretic mobility measurements for samples were collected using a Zetasizer Nano ZS instrument (Malvern Instruments, Inc., Southborough, MA), with reproducibility verified by performing five repeat measurements. The self-optimization routine (laser attenuation and data collection time) in the Zetasizer software was used for all measurements. The zeta potential was calculated from the electrophoretic mobility using the Henry equation. The solutions were prepared by dissolving nanoparticles in a concentration of 0.5 g/L for the characterizations. HCl was used to dissolute the $Ru(OH)_3$ shell of Ru/$Ru(OH)_3$ nanoparticles, then, the zeta potential of Ru nanoparticles can be measured. The content of Ru^{3+} in the centrifugal liquid was measured by an OPTIMA 2000 inductively coupled plasma optical emission spectrometer (ICP-OES) (PerkinElmer Co.).

2.5. Activity Test of Catalysts. The activity tests for catalytic oxidation of ethanol over the Ru supported catalysts were carried out in a fixed-bed quartz flow reactor (4 mm i.d.) containing approximately 50 mg of catalyst (60−80 mesh) in all the experiments. The reactor was heated by a temperature-controlled furnace. A thermocouple was placed on the outside of the reactor tube. The reaction mixture consisted of 1000 ppm ethanol and 20% O_2 in N_2, was fed at a rate of 50 mL min^{-1}. The 1000 ppm ethanol gas was produced by a high-purity nitrogen stream bubbling through a saturator filled with liquid ethanol. The reactants and the products such as ethanol, acetaldehyde, and CO_2 were analyzed online using a gas chromatograph equipped with a Porapak Q column (Agilent 6890N). At each reaction temperature, the reaction system was kept for 2.5 h to reach a steady state before analysis of the product.

3. Results and Discussion

3.1. Fabrication of Ru/RuO_2 Core−Shell Nanoparticles. *3.1.1. Electrochemical Synthesis of Ru Nanoparticles.* Homogeneously dispersed Ru nanoparticles were synthesized electrochemically in a potentiostatic manner. All experimental details are supplied in the Experimental Section. When the potential of working electrode vs a saturated calomel electrode (SCE) exceed to 0.2 V, the Ru^{3+} was oxidized to RuO_2 or RuO_3. On the contrary, when the potential is lower than 0.2 V, Ru^{3+} was reduced to Ru^{2+} or Ru.

Figure 1a shows the cyclic voltammetries (CV) of the behavior of ruthenium ions and its oxides on the Pt electrode in the potential window of −1.2 to 1.6 V vs SCE, and Figure 1b shows the reduction of Ru^{3+} to Ru in the potential window of −1.0 to 0.2 V vs SCE. As shown in Figure 1a, the potential of the peaks at approximately 0.2 and 0.8 V vs SCE were in response to the reduction of RuO_2 to Ru^{3+} and RuO_3 to RuO_2, respectively.[7] The reduction of Ru^{3+} to metallic Ru requires two steps on the platinum disk: the reductions of Ru^{3+} to Ru^{2+} and Ru^{2+} to Ru. Figure 1b shows that CV cathodic scans yielded a reduction peak at about −0.4 V, and the corresponding anodic reverse scan showed the counter peak at −0.375 V, which are in response to the redox peaks of Ru^{3+}/Ru^{2+} (the standard electrode potential of Ru^{3+}/Ru^{2+} is 0.249 V in 1 M H^+ aqueous solution[8]). The Ru^{2+} was reduced to

(6) Zhou, K.; Wang, X.; Sun, X.; Peng, Q.; Li, Y. *J. Catal.* **2005**, *229*, 206–212. Liu, X.; Zhou, K.; Wang, L.; Wang, B.; Li, Y. *J. Am. Chem. Soc.* **2009**, *131*, 3140–3141.

(7) Kumar, A. S.; Tanase, T.; Zen, J. *Langmuir* **2009**, *25*(23), 13633–13640.

(8) Dean, J.A., *Lange's Handnook of Chemistry*, 15th ed.; McGraw-Hill: New York, 1999.

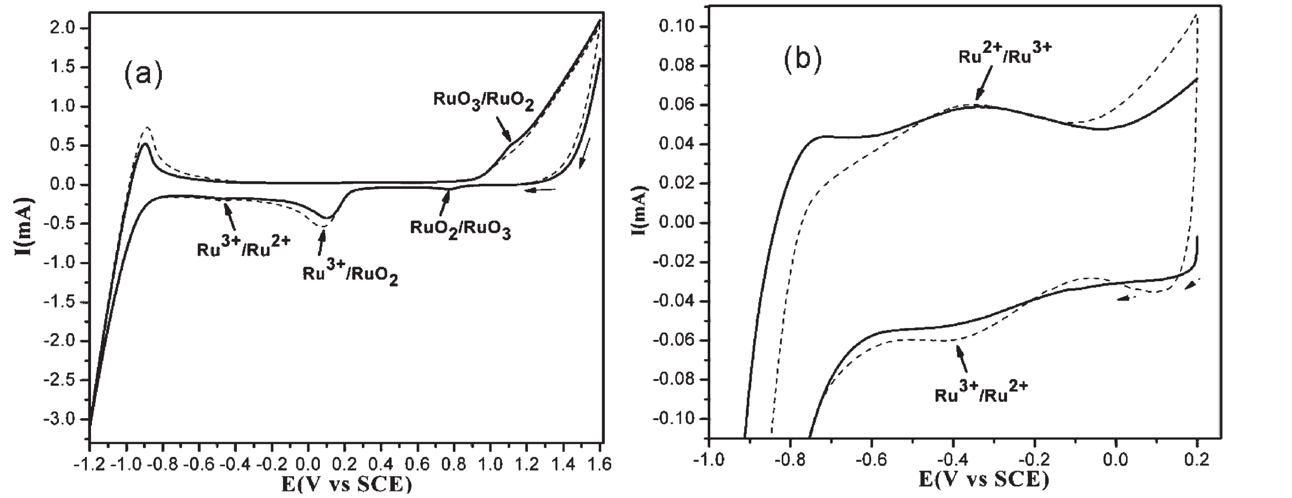

Figure 1. Cyclic voltammograms of the behavior of ruthenium ions and its oxides in the potential window of (a) −1.2 to 1.6 V vs SCE, and (b) −1.0 to 0.2 V versus SCE. Conditions: scan rate 20 mV s^{-1}, electrolyte was 5.0 × 10^{-4} mol L^{-1} $RuCl_3$ and 0.1 mol L^{-1} KNO_3; the solid line and dotted line represent the first and the 20th cycle, respectively.

metallic Ru at a potential between −0.4 V and −0.9 V, according to the results of the reference on cathodic deposit of Ru at the potential −0.9 V.[9] In addition, Figure 1 shows that the hydrogen evolution occurred at a potential more negative than −0.9 V. As the applied potential on the working electrode was −1.0 V versus SCE, the reduction of Ru^{3+} to Ru was accompanied with the hydrogen evolution.

3.1.2. Formation of RuO_2. During electrolysis, the pH of the electrolyte increased from 3.16 to 3.26. The color of the electrolyte changed from brown (the color of the Ru^{3+} solution) to nearly colorless, indicating the cessation of the electrochemical synthesis of nanoparticles. The 2.0 × 10^{-5} mol L^{-1} Ru^{3+} content in the centrifugal liquid indicated that 96% of the Ru^{3+} was converted into nanoparticles. Considering the 1 × 10^{-36} K_{sp} of $Ru(OH)_3$,[8] $Ru(OH)_3$ could be formed during the electrochemical synthesis when the pH value of the solution is higher than 3.19 and the concentration of Ru^{3+} in solution is at the level of 1 × 10^{-5} mol L^{-1}. The reason for the $Ru(OH)_3$ covering the Ru nanoparticles will be discussed later. The fresh dendritic Ru/$Ru(OH)_3$ nanoparticles float on water (Figure 2A). When all dendritic Ru/$Ru(OH)_3$ nanoparticles were centrifuge-washed and dispersed in 40 mL water ultrasonically in atmosphere, the $Ru(OH)_3$ were oxidized by O_2 to hydrated RuO_2. A transparent and homogeneous solution formed (Figure 2B), whose weight content was 3.6 × 10^{-2} g L^{-1} calculated by atomic Ru. This result indicated that the physical aggregation of the fresh nanoparticles was readily disrupted by the dilution and sonication. The solution remained transparent for 3 days with no visible coagulation (Figure 2C).

3.2. Characterization of Ru/RuO_2 Core−Shell Nanoparticles. Transmission electron microscopy (TEM) images showed that the highly monodispersed Ru/RuO_2 nanoparticles were spherical in shape and narrow in size distribution of Ru cores (average diameter of 1.95 nm), as can be seen

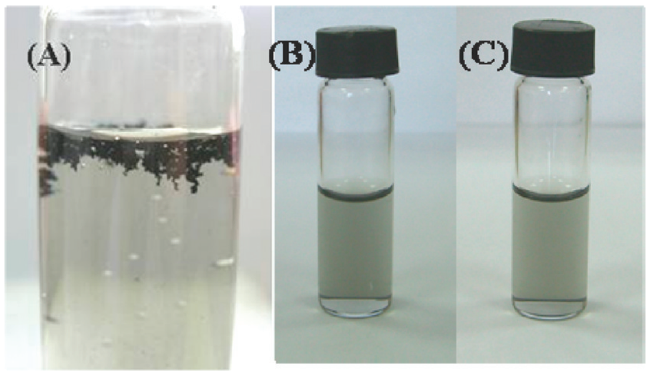

Figure 2. Images of (A) freshly accumulated Ru/$Ru(OH)_3$ nanoparticles in water, (B) Ru/RuO_2 nanoparticles after 10 min of ultrasonic dispersion in 40 mL water, and (C) monodispersed Ru/RuO_2 nanoparticles in solution after refrigeration for 3 days.

from Figure 3a. Compared to the shell, the Ru core was darker because of the difference in electron penetration efficiency (Figure 3b).[10] High-resolution TEM images of the Ru/RuO_2 core−shell nanoparticles (inset of Figure 3b) showed that the Ru core is a single crystal with visible lattice fringes at a spacing of 0.24 nm, which is in good agreement with the 0.234 nm spacing of the (1000) plane for the hexagonal closest-packed Ru [X-ray powder data file JCPDS no. 06−0663], whereas RuO_2 shell is amorphous. After total reduction of Ru/RuO_2 by bubbling with hydrogen for 24 h, the solution was sealed at room temperature for 24 h. The sample was then measured by TEM (Figure 3c). It is clear that the RuO_2 shell was completely reduced to Ru and the Ru nanoparticles greatly grew up and aggregated, confirming that reduced Ru nanoparticles are not stable in water in the absence of stabilizers. It is well-known that the noble nanoparticles prefer aggregating in water owing to their high surface energy. Ru/RuO_2 can be dispersed and stable in water, which is probably due to the existence of the hydrophilic RuO_2 shell. Energy-dispersive spectroscopy (EDS) data of the Ru/RuO_2 nanoparticles indicate that the atomic ratio of Ru and O is close to 1 as shown in table 1.

(9) Jow, J.; Lee, H.; Chen, H.; Wu, M.; Wei, T. *Electrochim. Acta* **2007**, *52*, 2625–2633.

(10) Masala, O.; Seshadri, R. *J. Am. Chem. Soc.* **2005**, *127*, 9354–9355.

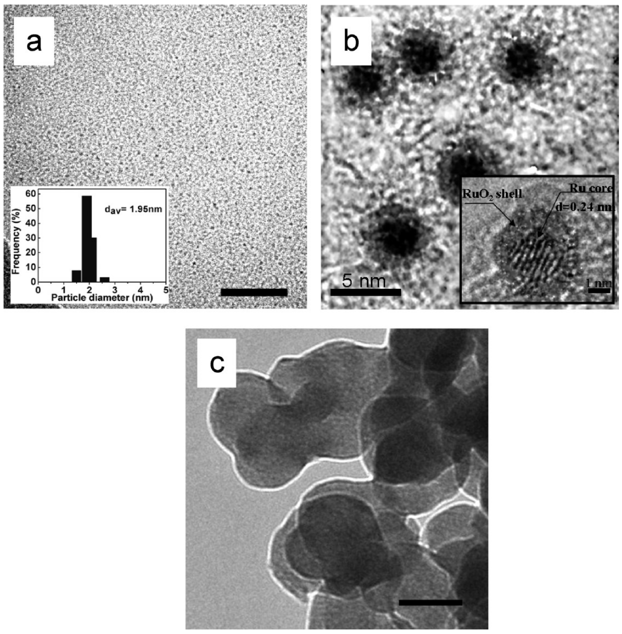

Figure 3. (a) TEM image of the Ru/RuO_2 nanoparticles, (b) core−shell structure and HRTEM image of Ru/RuO_2 nanoparticles, (c) TEM image of the reduced Ru/RuO_2 particles. The scale bar for TEM images is 50 nm in this paper.

Table 1. EDS Analysis of Ru/RuO_2 Nanoparticles on Copper Grid

characteristic X-ray (energy, $h\nu$ (keV))	at %	error %
C Kα (0.277)	44.01	0.01
O Kα (0.525)	13.79	0.15
Cu Kα (8.040)	28.76	0.08
Ru Lα (2.558)	13.44	0.11
Totals	100.0	

X-ray photoelectron spectroscopy (XPS) was performed to identify the nature of the Ru/RuO_2 nanoparticle surface. In Figure 4a, the peaks of the Ru $3d_{5/2}$ binding energy at about 280.8 and 280.1 eV corresponded well to the standard data of RuO_2 and Ru, respectively. The peaks at about 285.0 and 284.2 eV corresponded to the Ru $3d_{3/2}$ of RuO_2 and Ru, respectively. After Ar^+ bombardment of the sample (Figure 4b), the intensity of the peaks at 280.8 and 285.0 eV attributed to RuO_2 decreased sharply, which was accompanied by significant increases in the intensity of the Ru peaks at 280.1 and 284.2 eV. This implies that the Ar^+ beam partially removed the RuO_2 shell, resulting in an increase in the ratio of Ru/RuO_2. These results give direct evidence to the coexistence of Ru core and RuO_2 shell in Ru/RuO_2 nanoparticle.

It is well-known that the net charge of nanoparticles is a key parameter for their stability in solution.[11] The zeta potential represents the degree of repulsion between charged adjacent nanoparticles in dispersion. The general rule for ensuring electrostatic stability of particles is that the absolute value of zeta potential should not be less than 30 mV.[12] As shown in Figure 5, the zeta potential of the fresh nanoparticles prepared by our method was 30.8 mV

(11) Wikipedia, the free encyclopedia. http://en.wikipedia.org/wiki/Zeta_potential
(12) Deluca, T.; Kaszuba, M.; Mattison, K. *Am. Lab.* (June/July), 2006. Online Available: http://www.malvern.co.uk/common/downloads/campaign/mrk804-01.pdf.

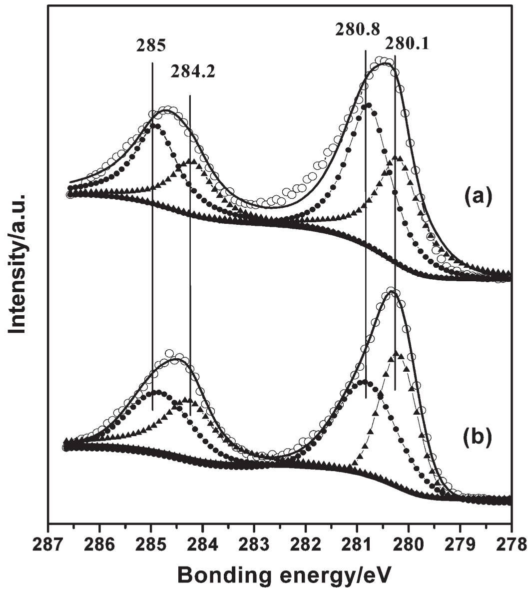

Figure 4. (a) XPS spectra of Ru 3d for Ru/RuO_2 nanoparticle; (b) XPS spectra of Ru 3d measured after Ar^+ bombardment (1×10^{-5} Torr Argon, 500 eV, 2 min) at 298 K. The circle is the actual experimental data; the thin lines are the fitted curves; the thick lines curves are the baselines fitted by the Shirley function. (▲) represents Ru^0 and (●) represents Ru^{4+}.

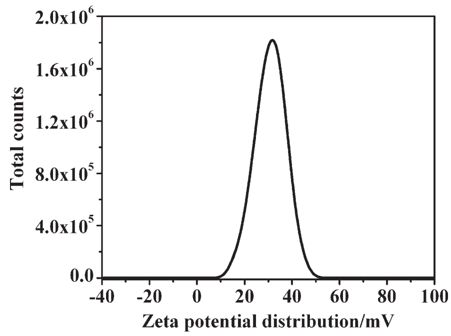

Figure 5. Zeta potential distribution of Ru/RuO_2 nanoparticles in water.

(in pure water at 25 °C). Therefore, Ru/RuO_2 nanoparticles hold enough electrostatic repulsion to prevent agglomeration, which is the main reason why the Ru/RuO_2 nanoparticles are stable in aqueous solution without stabilizer protection. In contrast, the zeta potential of the reduced Ru nanoparticles is about −4 mV (the measurement procedure was described in the Experimental Section), so the reduced Ru nanoparticles aggregate.

3.3. Mechanism of the $Ru/Ru(OH)_3$ Formation. On the basis of the results above, we proposed two possible pathways for the $Ru/Ru(OH)_3$ formation; the scheme is shown in Figure 6. One is that the Ru^{3+} first adsorbs on the surface of Ru nanoparticles and then reacts with OH^- to form $Ru(OH)_3$. The zeta potential of Ru nanoparticles was measured to be −4 mV, indicating that a negative charge dispersed on the surface of Ru nanoparticles, which made Ru nanoparticles favorable to adsorb cations. Moreover, the Ru^{3+} concentration around the cathode was comparatively high due to the mobility of Ru^{3+} in the electric field. When the Ru nanoparticles transferred from the cathode to the solution, Ru^{3+} could simultaneously adsorb on the surface of the Ru nanoparticles by Coulomb attraction. As the

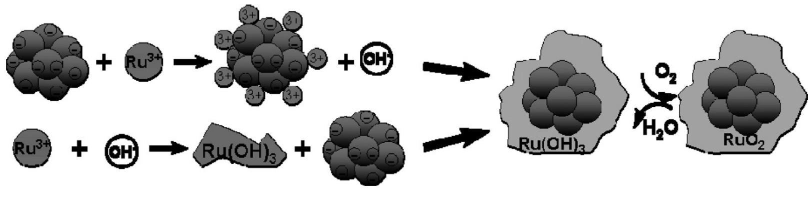

Figure 6. Formation of a Ru/RuO_2 core–shell nanoparticle.

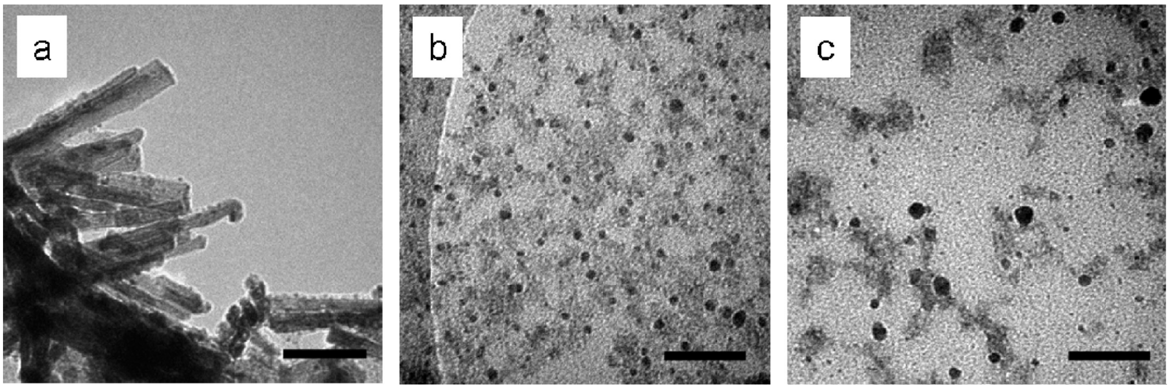

Figure 7. TEM images of 1 wt % Ru–supported catalysts: (a) Ru/CeO_2, (b) Ru/TiO_2, (c) Ru/Al_2O_3.

applied potential on the working electrode was −1.0 V versus SCE, the occurrence of hydrogen evolution resulted in an increase in pH levels. When the pH value of the solution was higher than 3.19, $Ru(OH)_3$ could be formed. The other possible process is that the $Ru(OH)_3$ is first formed in solution accompanied with hydrogen evolution and then covers the Ru nanoparticle. Finally, $Ru(OH)_3$ was oxidized into RuO_2 by O_2 with centrifuge-washing and ultrasonic dispersion in 40 mL of water in atmosphere.

3.4. Activity of Ru/RuO_2-Supported Catalysts. We further loaded this kind of Ru/RuO_2 nanoparticle onto support. Here, three common supports, CeO_2, TiO_2, and Al_2O_3, were employed. The preparation procedure was described in the Experimental Section. The morphologies of supported Ru/RuO_2 catalysts are shown in Figure 7. Obviously, the size of the Ru/RuO_2 nanoparticles was significantly influenced by the supports. The average diameter of the nanoparticles was 2.0 nm, 4.0 nm, and 5.0 nm on the CeO_2, TiO_2, and Al_2O_3 supports, respectively (200−250 particles were counted to evaluate the average size of particle). The different interactions between the Ru/RuO_2 nanoparticles and supports possibly account for the size difference of loaded nanoparticles.[1a,13−15] The XRD profiles of catalysts were shown in Figure 8. There were no diffraction peaks of Ru and RuO_2 on 1 wt % Ru/CeO_2(re) and 1 wt % Ru/TiO_2(re), even on 2 wt % Ru/CeO_2(re) catalyst, whereas the RuO_2 diffraction peak appeared on 0.5 wt % Ru/Al_2O_3(re) catalyst. The results indicated the Ru/RuO_2 nanoparticle is highly dispersed on CeO_2 and TiO_2. Moreover, the structure of Ru core and RuO_2 shell remained unchanged on CeO_2 support in 3 wt % Ru/CeO_2 (re) catalyst, whereas the Ru core was oxidized to RuO_2 on TiO_2 and Al_2O_3. According to the results above, CeO_2 is a suitable support for loading Ru and/or RuO_2 nanoparticles. In addition, the appearance of the crystalline RuO_2 on the supported catalysts indicated that the high-temperature treatment during the loading process resulted in the crystallization of amorphous RuO_2 shell (shown in Figure 3b). To load the narrow-sized nanoparticles in solution to support is always a challenge during the preparation of well-defined supported catalyst. One of the issues is the removal of the stabilizer whose residual generally result in the decrease of the catalyst activity. Our synthetic strategy provides a promising method to prepare the supported Ru and/or RuO_2 catalyst without interruption by stabilizers or/and anions.

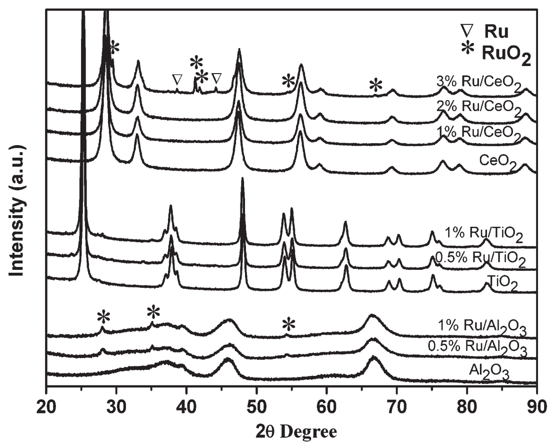

Figure 8. XRD data of Ru/Al_2O_3(re), Ru/CeO_2(re), and Ru/TiO_2(re) catalysts with different Ru loadings.

The catalytic oxidation of ethanol was chosen to examine the catalytic properties of the Ru/RuO_2 nanoparticles supported catalysts. The activities of the Ru/RuO_2

(13) Zheng, N.; Stucky, G. D. *J. Am. Chem. Soc.* **2006**, *128*, 14278–14280.
(14) Esch, F.; Fabris, S.; Zhou, L.; Montini, T.; Africh, C.; Fornasiero, P.; Comelli, G.; Rosei, R. *Science* **2005**, *309*, 752–755.
(15) Comotti, M.; Li, W. C.; Spliethoff, B.; Schüth, F. *J. Am. Chem. Soc.* **2006**, *128*, 917–924.

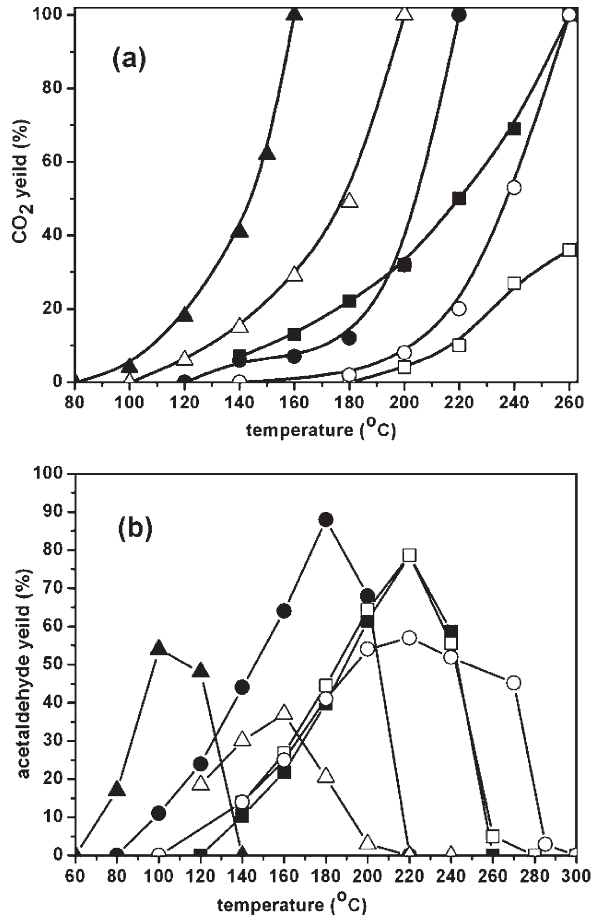

Figure 9. Comparison of catalytic activity for (a) complete oxidation of ethanol to CO_2 and (b) selective oxidation of ethanol to acetaldehyde. Reaction conditions: 50 mg of catalyst, 1000 ppm ethanol, gas hourly space velocity (GHSV) of 60 000 h^{-1}. (▲)Ru/CeO_2(re), (●)Ru/TiO_2(re), (■)Ru/Al_2O_3(re), (△)Ru/CeO_2(im), (○) Ru/TiO_2(im), (□) Ru/Al_2O_3(im).

nanoparticles supported catalysts were compared with that of the catalysts prepared by $RuCl_3$ wet impregnation. As shown in Figure 9, all catalysts prepared by loading Ru/RuO_2 nanoparticles on supports showed much higher catalytic activity than the catalysts prepared by wet impregnation method. For example, 1% Ru/CeO_2 (re) prepared by loading Ru/RuO_2 nanoparticles exhibited 100% ethanol conversion to CO_2 at 160 °C, while the temperature of the same ethanol conversion on 1% Ru/CeO_2(im) is 200 °C which is similar to the previously reported results.[1a] Moreover, the complete oxidation of ethanol with time-on-stream at 160 °C was studied on 1% Ru/CeO_2(re) (Figure 10). Clearly, its complete conver-

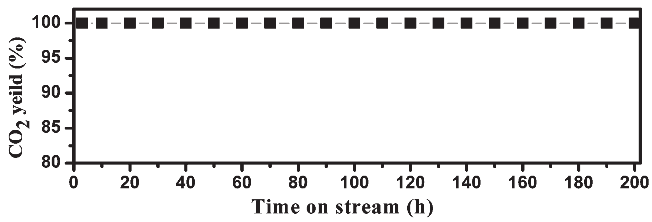

Figure 10. CO_2 yield with time on stream over the 1% Ru/CeO_2 catalyst. Catalysis conditions: reaction temperature = 160 °C, 50 mg of catalyst, 1000 ppm ethanol, GHSV of 60 000 h^{-1}.

sion of ethanol into CO_2 remained unchanged and no deactivation of catalytic activity was observed, even after 200 h time-on-stream, indicating that the Ru/CeO_2 catalyst is relatively stable under an ethanol oxidation atmosphere at 160 °C. In comparison, the Ru/TiO_2 catalyst showed a prominent activity for the selective catalytic oxidation of ethanol with 88% acetaldehyde yield at 180 °C (Figure 9b), which is unusual for catalysts in gas−solid conditions. The mechanism of the ethanol oxidation on Ru/RuO_2 supported catalysts need to be further researched.

4. Conclusions

Ru/RuO_2 core−shell nanoparticles were first synthesized by electrochemical method in water without the addition of stabilizers. Ru/RuO_2 nanoparticles possess enough electrostatic repulsion to prevent agglomeration, which is the reason for the stability of Ru/RuO_2 nanoparticles in water without addition of stabilizers. The successful synthesis of "unprotective" Ru/RuO_2 core−shell particles provides new opportunities in the preparation of catalysts or functional materials containing Ru and its oxides. All Ru/RuO_2-nanoparticle-supported catalysts showed higher catalytic activity for the oxidation of ethanol than the catalysts prepared by traditional wet impregnation method. Among them, 1 wt % Ru/CeO_2-(re) exhibited 100% ethanol conversion to CO_2 at 160 °C and no deactivation was observed even after 200 h time-on-stream. In view of the excellent activities of the Ru/RuO_2 catalysts for oxidation of ethanol, we believe that the unique structural properties of Ru nanostructures make them potentially applicable for catalysis.

Acknowledgment. This work was financially supported by the National Basic Research Program of China (2010CB-732304) and the National High Technology Research and Development Program of China (2007AA061402).